metals

MDPI

Article

Structural Evolution of Nano-sized Oxide Particles Formed in Mechanically Alloyed Fe-10Cr-5Y_2O_3 Powders

Ga Eon Kim, Tae Kyu Kim and Sanghoon Noh *

Nuclear Materials Development Division, Korea Atomic Energy Research Institute, Daejeon 305-353, Korea; gaeonkim02@gmail.com (G.E.K.); tkkim2@kaeri.re.kr (T.K.K.)

* Correspondence: shnoh@kaeri.re.kr; Tel.: +82-42-868-4504

Received: 8 January 2020; Accepted: 24 February 2020; Published: 27 February 2020



Abstract: Fe-10Cr-5Y_2O_3 powders were mechanically alloyed using a high energy horizontal ball-mill apparatus, and the effect of heat treatment on the behavior of nano-sized oxide particles formed in the mechanically alloyed Fe-10Cr-5Y_2O_3 powders was investigated. Elongated Cr-rich and Y-rich oxides were observed in the mechanically alloyed powders. During the heating of these powders above 700 °C, the elongated Cr-rich oxides were dramatically changed to a near- spherical morphology. Cubic-Y_2O_3, monoclinic-Y_2O_3 and $YFeO_3$ phases were also found after heat treatment at 1150 °C for 1h, indicating that the Y-rich oxide phase was transformed to the cubic-Y_2O_3, monoclinic-Y_2O_3 and $YFeO_3$ ones. It is thus concluded that both a morphological change of Cr-rich oxide and a phase transformation of Y-rich oxide during the heating of mechanically alloyed powders could be mainly attributed to extremely high energy, accumulated by the mechanical alloying process.

Keywords: oxide dispersion strengthening (ODS); oxide particle; Cr-rich oxide; Y-rich oxide

1. Introduction

Oxide dispersion strengthened (ODS) steels have an excellent irradiation resistance and superior high-temperature mechanical properties [1,2]. Compared to commercial steels, the additionally improved irradiation resistance and mechanical properties of ODS steels come from the presence of nano-sized oxide precipitates in the matrix [3]. For several decades, ODS steels have been developed as fuel cladding tube materials for sodium-cooled fast reactors (SFR). Recently, a 10 wt.% Cr ODS ferritic/martensitic steel with some minor elements has been newly developed for the in-core structural components of SFR, which has very attractive microstructures to achieve both superior creep and radiation resistances at high temperatures [1,4]. The oxide particles in the matrix act as sinks for defects such as helium bubbles, delay the nucleation of large voids and act as obstacles for the dislocation movement at high temperatures under neutron irradiation environment [5]. The characteristics of ODS steels are mainly decided by the size, inter-spacing and the crystallographic relationship with the matrix of oxide particles [6]. In order to enhance the performance of ODS steels, the oxide particles should be a few nanometers in size and need to be homogeneously distributed in the matrix. The mechanical alloying (MA) process is one of the essential methods to fabricate the ODS steels. In this process, the continuous collision between hard grinding media and raw powders with a high revolving energy causes the repeated crushing and cold welding of powders. This eventually creates the uniform alloy and the dispersion of oxide particles in the steel matrix [7]. As the major strengthening phase, Y_2O_3 particles are regular appended to the Fe-Cr matrix. Since the properties of ODS steels depend on the dispersion of nano-sized oxide, controlling their nucleation and growth during the manufacturing process is essential, but is difficult in the standard production method. Depending

upon the chemical composition, the consolidation techniques and various kinds of oxides have been reported in the literature [8–10]. However, a detailed study of Y_2O_3 particles during the manufacturing route still needs to be elucidated. It is known that the mechanism of nano-sized oxide formation is a dissolution of Y_2O_3 during ball milling followed by the precipitation of oxides during subsequent annealing [11,12]. Theoretical predictions exist for the mechanism of oxide particle formation based on experimental results, but additional study into the stage of nano-sized oxide particle formation is necessary. In this study, as a part of the new development of 10Cr wt.% ODS ferritic/martensitic steel for the in-core structural components of the SFR, the microstructural evolutions of nano-scaled oxide particles were investigated during the hot consolidation process. A model alloy powder composed of Fe(bal.)-10Cr-5Y_2O_3 in wt.% were mechanically alloyed, and subsequent heating processes were implemented. In-situ electron microscopy and crystallographic analysis were intensively employed.

2. Materials and Methods

Pure Fe, 10wt.% Cr and 5wt.% Y_2O_3 powders were mechanically alloyed, followed by heat treatment at 1150 °C. The Fe and Cr powders in the size range of 50–120 μm and Y_2O_3 powders in the size range of 20–40 nm were mechanically alloyed using a high energy horizontal ball-mill apparatus (Simoloyer CM20, Zoz Inc., Wilstedt, Germany) at 300 rpm, with a ball to powder ratio of 10:1 for 48 h in an argon gas atmosphere. The mechanically alloyed Fe-10Cr-5Y_2O_3 powders were heated up to 900 °C in a high vacuum. In addition, heat treatment at 1150 °C for 1 h was also carried out. The particle size, morphology and composition distribution of mechanically alloyed powders were observed using Scanning Electron Microscopy (SEM, JSM-6300, JEOL Inc., Tokyo, Japan) and Electron Probe Microanalysis (EPMA, JXA-8500FK, JEOL Inc.,Tokoy, Japan). The microstructure was characterized by High resolution Transmission Electron Microscopy (TEM, JEM-2100F, JEOL Inc., Tokyo, Japan) with an acceleration voltage of 200 kV. The samples for TEM observation were prepared by mechanically polishing to a thickness range of 50–70 μm and then twin-jet electro polishing in 10% methly-alcohol and 90% perchloric acid solution in vol.% at −40 °C with 25 V. The crystal structures of Fe-10Cr-5Y_2O_3 powders before MA, after MA and heat treated at 1150 °C, were investigated by using an X-ray Diffractometer (XRD, Ultimun IV, RIGAKU Inc., Tokyo, Japan). The diffraction patterns were collected over a 2θ range of 20–80° with a step width of 0.01°. The in-situ TEM study was performed at 200 kV with a Cs-corrector. The microstructure under different temperatures in mechanically alloyed Fe-10Cr-5Y_2O_3 powders in the range of 25–900 °C was examined by in-situ TEM with Energy Dispersive X-ray Spectroscopy (EDS). The samples for in-situ TEM analysis were prepared using the Focused Ion Beam (FIB) method. HRTEM, Selected Area Diffraction (SAD) patterns and Fast Fourier Transformation (FFT) images were evaluated to identify the crystal structure of nano-sized oxide particles and their crystallographic orientation relationship with the matrix [13,14].

3. Results and Discussion

3.1. Microstructure of Mechanically Alloyed Powders

Figure 1 shows the SEM and EPMA images of the mechanically alloyed Fe-10Cr-5Y_2O_3 powders. The mean diameter of mechanically alloyed powders was determined to be about 10 μm. In the mechanically alloyed Fe-10Cr-5Y_2O_3 powders, it was observed that the Fe, Cr, Y and O elements were uniformly distributed inside the powder. It appears that the Fe, Cr, Y_2O_3 elements are finely dispersed inside the matrix and reached a super-saturated solid solution in 48 h. During the MA process, work hardening was introduced into the ductile Fe and Cr, and brittle Y_2O_3 powders, and the particle size became smaller than in raw powders. The mechanically alloyed Fe-10Cr-5Y_2O_3 powders showed the typical features of severe plastic deformation, which was ascribed to the repeated fracture and cold-welding of the powder mixture. It is indicated that MA creates a high density of crystal defects such as dislocations and grain boundaries.

Figure 2 shows the results of the microstructural observation of mechanically alloyed Fe-10Cr-5Y_2O_3 powder during the MA processing of the Fe, Cr and Y_2O_3 elements. The TEM image exhibits a complicated contrast. The SAD patterns seen in Figure 2b show that the outer rings coincide with Fe(110), Fe(200), Fe(211), Fe(310) and Fe(222). The SAD pattern of mechanically alloyed Fe-10Cr-5Y_2O_3 powder depicts only the nano-crystalline structure of α-Fe, and no ring corresponding to crystalline Y_2O_3 is observed. These results indicate that the raw Y_2O_3 particles were severely fragmented to ultrafine crystalline form and almost dissolved into the matrix by high energy forces during the MA process. The continuous diffraction spots imply that the crystalline size was further decreased and there were a lot of α-Fe grains at the nanoscale with random crystallographic orientations within a particle. The HRTEM image of mechanically alloyed Fe-10Cr-5Y_2O_3 powders show that no lattice fringe area was analyzed (Figure 2c). It is indicated that the ultrafine crystalline Y_2O_3 particles were located in the grain boundaries of α-Fe grains. An obvious diffraction contrast for the Y_2O_3 of a FFT image was not acquired as shown in Figure 2d. The MA process generated grain boundaries, and the nano-crystalline oxide particles should be isolated on the grain boundaries.

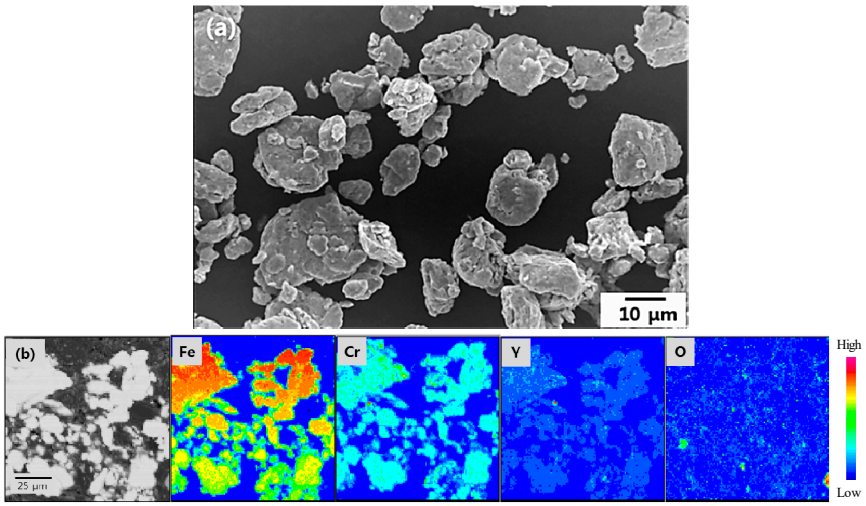


Figure 1. SEM (Scanning Electron Microscopy) and EPMA (Electron Probe Microanalysis) images of the mechanically alloyed Fe-10Cr-5Y_2O_3 powders: (**a**) SEM and (**b**) EPMA mapping images.

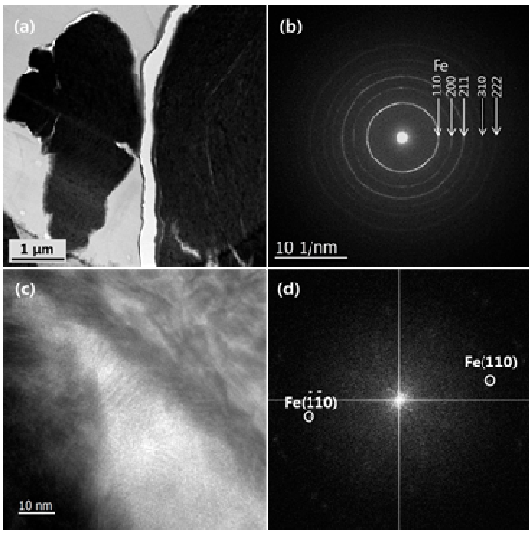


Figure 2. TEM (Transmission Electron Microscopy) analysis results of the mechanically alloyed Fe-10Cr-5Y_2O_3 powders: (**a**) TEM image, (**b**) SAD (Selected Area Diffraction) pattern, (**c**) HRTEM (High Resolution Transmission Electron Microscopy) image, and (**d**) FFT (Fast Fourier Transformation) pattern.

Figure 3 shows the microstructure of mechanically alloyed Fe-10Cr-5Y_2O_3 powder after heating at 900 °C using in-situ TEM. The TEM image indicates that the grain growth occurred as shown in Figure 3a. The SAD pattern in Figure 3b shows that the powder was polycrystalline, and a diffraction ring corresponding to Y_2O_3(222) was detected. On heating, the continuous ring is changed to a discontinuous ring, and a crystalline spot of oxide particle also appears. The lattice parameter of the matrix was determined from the SAD patterns to be about 0.2038 ± 0.005 nm. The HRTEM image of mechanically alloyed Fe-10Cr-5Y_2O_3 powders after heating at 900 °C is presented in Figure 3c. The area of lattice fringes is clearly observed. The FFT analysis results show that the Y_2O_3-type structure in the matrix was determined, as shown in Figure 3d. The measured major directions correspond to $d_{(411)}$ (2.48Å), $d_{(222)}$ (3.07Å) and $d_{(213)}$ (2.86Å). When the mechanically alloyed Fe-10Cr-5Y_2O_3 powder was heated from 25 °C to 900 °C, nano-crystalline oxide particles might have been precipitated in the matrix. Although the crystal structure of oxide particle was observed by the SAD pattern, the obvious shape and size of oxide particles was not investigated.

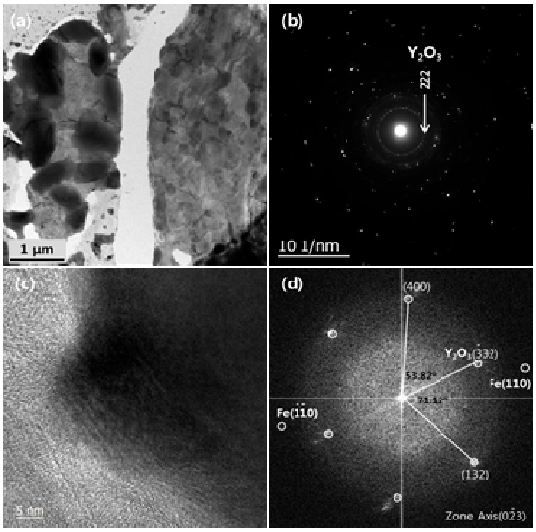


Figure 3. TEM analysis results of mechanically alloyed Fe-10Cr-5Y_2O_3 powders after heat treatment at 90 °C: (**a**) TEM image, (**b**) SAD pattern, (**c**) HRTEM image, and (**d**) FFT pattern.

3.2. Microstructural Evolution of Oxide Particles

Figure 4 shows the microstructural observation of temperature-dependent phenomena in mechanically alloyed Fe-10Cr-5Y_2O_3 powder up to 900 °C. A nano-crystalline textured structure was observed in the mechanically alloyed powder before heating (Figure 4a). It was revealed that the microstructure of mechanically alloyed powder was a nano-crystalline textured structure. There were no significant changes to the microstructure until the temperature reached up to 600 °C (Figure 4b). A further increase in temperature caused significant changes in the microstructure. Upon heating above 700 °C (Figure 4c), grain growth of the crystalline phase was detected. During heating from 800 °C to 900 °C (Figure 4d,e), considerable grain growth of nano-sized oxide particles occurred. Consequently, the nano-sized particle grew to a few microns in diameter after heating at 900 °C, as shown in Figure 4f. Based on these results, the nano-sized grain and tangled dislocations were initially produced by the MA process. It may have caused the transfer of mechanical energy to the powder particles and led to the introduction of strain into the powders through the generation of dislocations and other defects, which act as fast diffusion paths. The heating process induced a microstructural change accompanied with grain coarsening, diffusion and the re-distribution of refined particles. The results demonstrate that crystallization of the nano-crystalline structure occurred at about 900 °C, based on the SAD pattern analysis result.

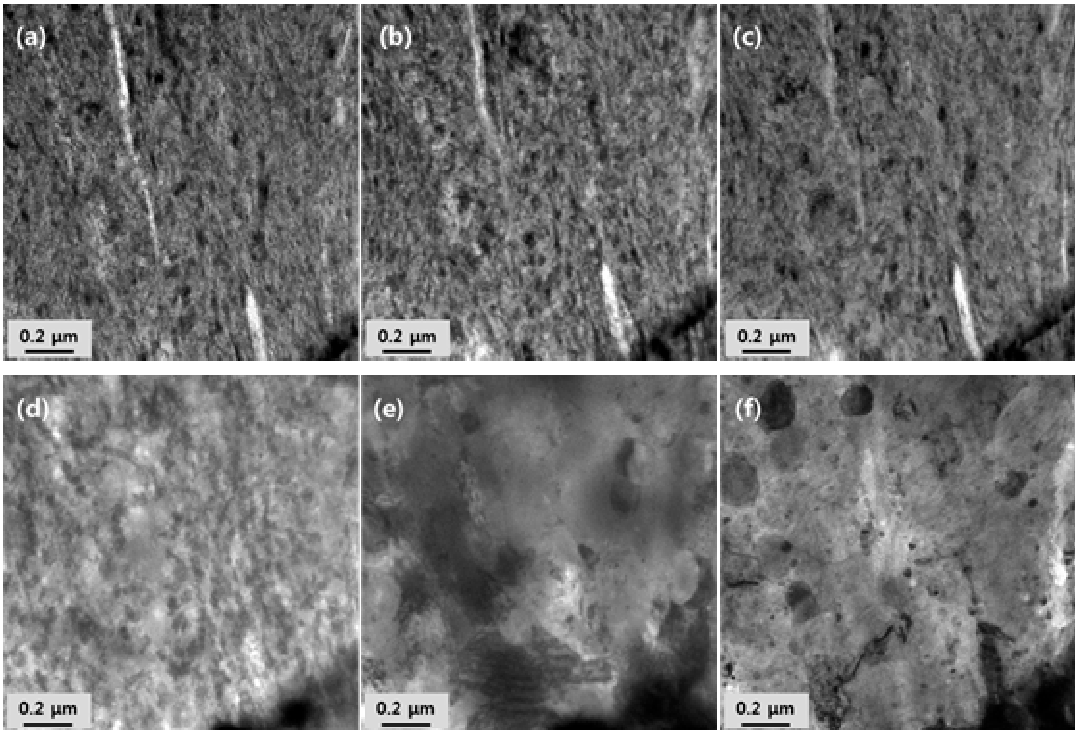


Figure 4. In-situ TEM images of the mechanically alloyed Fe-10Cr-5Y_2O_3 powders after heating at (**a**) 25 °C, (**b**) 600 °C, (**c**) 700 °C, (**d**) 800 °C, (**e**) 900 °C and (**f**) after cooling from 900 °C to room temperature.

Figure 5 shows the TEM/EDS mapping images of Fe-10Cr-5Y_2O_3 powders after MA and heating at 900 °C. As shown in Figure 5a, the microstructure consisted of refined Cr-rich and Y-rich oxide particles dispersed and elongated within the nano-crystalline structure. It may be that the formation of solid solutions and the intermetallic phase by MA constitutionally changed the particles from equilibrium to supersaturated and metastable conditions. According to the TEM/EDS image, after heating at 900 °C, growth behavior similar to aggregation occurred on enrichment of the Cr, O and Y_2O_3 region (Figure 5b). The EDS mapping analysis confirmed that nano-scale particles coalesced to minimize the surface energy during the heating process. It was indicated that the heat energy was delivered into the particles through the grain boundary and released the stored energy in the materials. The site of Cr-rich and Y-rich oxide elements where the dislocation density remains much higher from 25 °C to 900 °C preferentially bonded to neighbor atoms like Fe, Cr, vacancy or excess oxygen. This is because the equilibrium shape of a particle was generally governed by the surface energy between the particle and the matrix. It is proposed that new oxide crystals nucleate on a special crystalline plane of the matrix and grow through surface diffusion with the minimization of surface energy, consequently leading to the formation of spherical or faceted particles. The localized formation of the metastable oxide particle then results from both the locally high super-saturation and interaction with the stabilizing matrix. Following the crystallization of nano-sized oxide particles, their interaction may lead to growth through either coarsening or aggregation, and coalescence. After heating, the TEM observations indicated that the particles were larger and that the morphological evolution of the oxide particles formed an aggregate shape assumed to be spherical for theoretical interpretation.

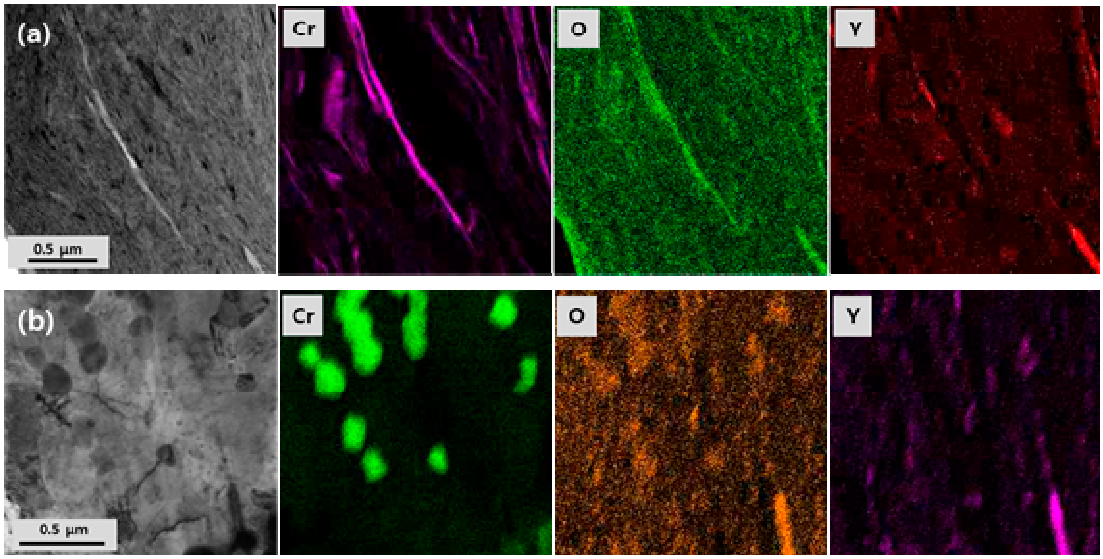


Figure 5. TEM/Energy Dispersive X-ray Spectroscopy (EDS) study results for the mechanically alloyed Fe-10Cr-5Y_2O_3 powders after: (**a**) MA and (**b**) heat treatment at 900 °C.

3.3. Crystal Structure

Figure 6 shows the XRD patterns of the Fe-10Cr-5Y_2O_3 powder before MA, after MA and after heat treatment at 1150 °C for 1 h. The Fe, Cr and Y_2O_3 peaks were clearly observed in the powders before the MA process, and the crystallite size of Y_2O_3 was measured to be in the range of 20–25 nm. It is interesting to notice that most of the Y_2O_3 peaks became broadened after MA. As a result, the crystallite size was reduced to the range of 13–16 nm. The reduction of Y_2O_3 peak intensities indicates that strong grain refinement occurred due to the high mechanical impact. It is considered that the reduction of Y_2O_3 peak intensities could be attributed to the strong grain refinement caused by the high mechanical impact during the MA process. These results assume that the Y_2O_3 phase corresponded to a Y-rich oxide phase. The result means that the Y_2O_3 phase is transformed to a Y-rich oxide phase during the MA process. However, cubic-Y_2O_3, monoclinic-Y_2O_3 and $YFeO_3$ diffraction peaks were observed in the heat treated powders. These results indicate that an extreme stored energy in the MA powders acts to cause the nucleation and growth of oxide particles during the heating process. This observation exhibits a good match with the TEM analysis results, indicating evidence of the evolution of the Y_2O_3 crystal structure. The variation of the Y_2O_3 peak proves the crystallization of the nano-sized oxide particles. The crystallite size was estimated to be in the range of 15–17 nm.

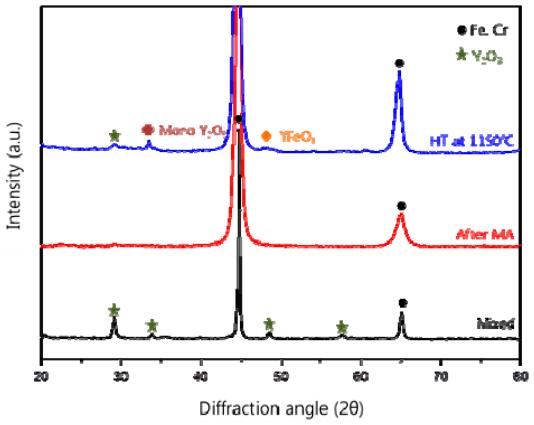


Figure 6. X-ray diffraction patterns of the Fe-10Cr-5Y_2O_3 powders before MA, after MA and after a heat treatment at 1150°C for 1 h.

Figure 7 shows the HRTEM study results for nano-sized Y_2O_3-type oxide particles in mechanically alloyed Fe-10Cr-5Y_2O_3 powder after heat treatment at 1150 °C for 1 h. The electron diffraction indicated that the inter-planar distances and angles were consistent with the (222) and the (400) crystallographic planes of Y_2O_3 in the zone axis for $d_{(222)}$ (3.06Å) and $d_{(400)}$ (2.63Å), with 53.7° between the planes. The orientation relationship between the Y_2O_3 particles (<10 nm) and the matrix turned out to be $(222)_{Oxide}//(220)_{matrix}$. On the basis of these observations, the HRTEM study results indicate that the nano-sized oxide particles had a structure consistent with a cubic-Y_2O_3 type, and the XRD analysis results show that new oxide particle structures were observed that were consistent with $YFeO_3$ and monoclinic-Y_2O_3 type particles. It is concluded that the stoichiometric Y_2O_3 phase is transformed to the non-stoichiometric Y_2O_3 structure during MA and that the nano-sized oxide particles of the $Y_\alpha Fe_\beta O_\gamma$-type structure are precipitated during heat treatment at high temperatures.

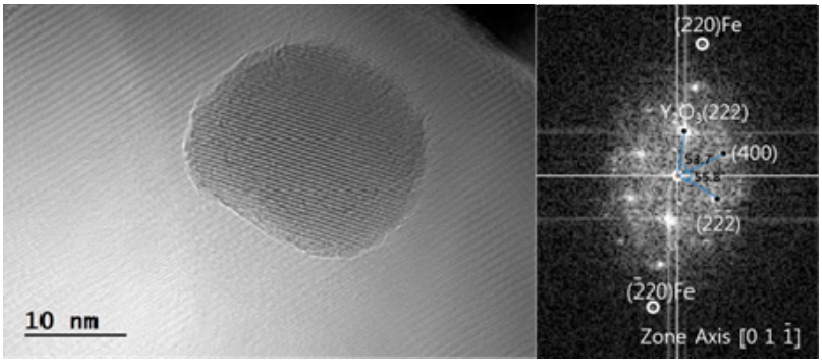


Figure 7. The HRTEM study results for Y_2O_3-type oxide particles in mechanically alloyed Fe-10Cr-5Y_2O_3 powder after heat treatment at 1150°C for 1 h.

4. Conclusions

Fe-10Cr-5Y_2O_3 powders were mechanically alloyed using a high energy horizontal ball-mill apparatus, and the behavior of oxide particles in the mechanically alloyed Fe-10Cr-5Y_2O_3 powders was evaluated. Two kinds of Cr-rich and Y-rich oxides were mainly observed in the elongated morphology. During the heating of mechanically alloyed powders above 700 °C, the elongated Cr-rich oxides were changed to a near-spherical morphology. After heat treatment at 1150 °C for 1 h, the cubic-Y_2O_3, monoclinic-Y_2O_3 and $YFeO_3$ phases were analyzed. This observation indicates that the Y-rich oxide phase in the mechanically alloyed powders is transformed to the cubic-Y_2O_3, monoclinic-Y_2O_3 and $YFeO_3$ ones. The precipitated Y_2O_3-type structure particle was consistent with the (222) and the (400) crystallographic planes of Y_2O_3 in the zone axis. The orientation relationship between the Y_2O_3 particles (<10 nm) and the matrix turned out to be $(222)_{Oxide}//(220)_{matrix}$. On the basis of these results, it is possible to summarize that both a morphological change of Cr-rich oxide and a phase transformation of Y-rich oxide during the heating of mechanically alloyed powders could be mainly attributed to extremely high energy accumulated by the mechanical alloying process.

Author Contributions: G.E.K. performed TEM investigation, methodology, and writing for original draft. T.K.K. performed conceptualization for this study, methodology, and support of the writing for original draft. S.N. performed SEM, EPMA investigation, heat treatment, and writing for review, editing. All authors discussed the results and contributed to manuscript. All authors have read and agreed to the published version of the manuscript.

Funding: This work was supported by the National Research Foundation of Korea (NRF) grant funded by the Korea government (MEST) (No. 2017M2A8A4017639).

Conflicts of Interest: The authors declare no conflict of interest.

References

1. Kim, T.K.; Noh, S.; Kang, S.H.; Park, J.J.; Jin, H.J.; Lee, M.K.; Jang, J.; Rhee, C.K. Current Status and Future Prospective of Advanced Radiation Resistant Oxide Dispersion Strengthened Steel (ARROS) Development for Nuclear Reactor System Applications. *Nucl. Eng. Technol.* **2016**, *48*, 572–594. [CrossRef]
2. Jin, H.J.; Kim, T.K. Neutron irradiation performance of Zircaloy-4 under research reactor operating conditions. *Ann. Nucl. Energy* **2015**, *75*, 309–315. [CrossRef]
3. Kim, T.K.; Noh, S.; Kang, S.H.; Jin, H.J.; Kim, G.E. Development of advanced radiation resistant ODS steel for fast reactor systems applications. *World J. Eng. Technol.* **2016**, *3*, 125–128. [CrossRef]
4. Kim, T.K.; Han, C.H.; Kang, S.H.; Noh, S.; Jang, J. Effects of oxygen concentration on the size distribution of oxide particles in ODS steel. *Curr. Nanosci.* **2014**, *10*, 94–96. [CrossRef]
5. Kim, T.K.; Bae, C.S.; Kim, D.H.; Jang, J.; Kim, S.H.; Lee, C.B.; Hahn, D. Microstructural observation and tensile isotropy of an austenitic ODS steel. *Nucl. Eng. Technol.* **2008**, *40*, 1–6. [CrossRef]
6. Noh, S.; Choi, B.K.; Kang, S.H.; Kim, T.K. Influence of mechanical alloying atmospheres on the microstructures and mechanically properties of 15Cr ODS steels. *Nucl. Eng. Technol.* **2014**, *46*, 857–862. [CrossRef]
7. Mao, X.; Oh, K.H.; Kang, S.H.; Kim, T.K.; Jang, J. On the coherency of Y2Ti2O7 particles with austenitic matrix of oxide dispersion strengthened steel. *Acta Mater.* **2015**, *89*, 141–152. [CrossRef]
8. Susila, P.; Sturm, D.; Heilmaier, M.; Murty, B.S.; Subramanya, V. Effect of yttria particle size on the microstructure and compression creep properties of nanostructured oxide dispersion strengthened ferritic (Fe-12Cr-2W-0.5Y2O3) alloy. *Mater. Sci. Eng. A* **2011**, *528*, 4579–4584. [CrossRef]
9. Srinivasan, D.; Corderman, R.; Subramanian, P.R. Strengthening mechanisms (via hardness analysis) in nanocrystalline NiCr with nanoscaled Y2O3 and Al2O3 dispersoids. *Mater. Sci. Eng. A* **2006**, *416*, 211–218. [CrossRef]
10. Sakasegawa, H.; Tamura, M.; Ohtsuka, S.; Ukai, S.; Tanigawa, H.; Kohyama, A.; Fujiwara, M. Precipitation behavior of oxide particles in mechanically alloyed powder of oxide-dispersion-strengthened steel. *J. Alloys Compd.* **2008**, *452*, 2–6. [CrossRef]
11. Kim, S.W.; Shobu, T.; Ohtsuka, S.; Kaito, T.; Inoue, M.; Ohuma, M. Kinetic approach for growth and coalescence of nano-size oxide particles in 9Cr-ODS steel using high-energy synchrotron radiation X-rays in SPring-8. *Mater. Trans.* **1993**, *204*, 65–73. [CrossRef]
12. Lescoat, M.L.; Ribs, J.; Chen, Y.; Marquis, E.A.; Bordas, E.; Trocellier, P.; Serruys, Y.; Gentils, A.; Kaitasov, O.; Carlan, Y.; et al. Radiation-induced ostwald ripening in oxide dispersion strengthened ferritic steels irradiated at high ion dose. *Acta Mater.* **2014**, *78*, 328–340. [CrossRef]
13. Brocq, M.; Radiguet, B.; Le Breton, J.M.; Cuvilly, F.; Pareige, P.; Legendre, F. Nanoscale characterization and clustering mechanism in an Fe-Y2O3 model ODS alloy processed by reactive ball milling and annealing. *Acta Mater.* **2010**, *58*, 1806–1814. [CrossRef]
14. London, A.J.; Santra, S.; Amirthapandian, S.; Panigrahi, B.K.; Sarguna, R.M.; Balaji, S.; Vijay, R.; Sundar, C.S.; Lozano-perez, S.; Grovenor, C.R.M. Effect of Ti and Cr on dispersion, structure and composition of oxide nano-particles in model ODS alloys. *Acta Mater.* **2015**, *97*, 223–233. [CrossRef]



© 2020 by the authors. Licensee MDPI, Basel, Switzerland. This article is an open access article distributed under the terms and conditions of the Creative Commons Attribution (CC BY) license (http://creativecommons.org/licenses/by/4.0/).